Seismic interferometry versus spatial auto-correlation method on the regional coda of the NPE

Sjoerd de Ridder

ABSTRACT

A seismic recording of the non-proliferation experiment (NPE) contains the first break of the regional P phases followed by a three minute long coda. The frequency-domain result of seismic interferometry is studied. This procedure is analogous to the spatial auto-correlation (SPAC) method, devised for studying microtremors by Aki (1957). Cross-correlating two receiver stations retrieves, under favorable circumstances, an approximation of the Green's function between these two stations. To first order, this Green's function consists of a direct event traveling between the receivers. In the frequency-domain, the lowest mode in the Green's function is a weighted and scaled zero-order Bessel function of the first kind, J_0. The cross-spectrum from the coda of the NPE is estimated using multi-taper spectral analysis. The retrieved Green's functions are fitted to damped J_0 functions to recover phase velocity and estimates of the attenuation coefficients. Only energy between 1-4 Hz can be fitted unambiguously with J_0 functions, because higher frequencies contain too much spurious energy. This result shows the equivalence of the SPAC method and seismic interferometry for the lowest mode in the Green's function. This study also demonstrates that the coda of a regional event, seemingly unfavorably positioned, can contain energy useful for seismic interferometry.

INTRODUCTION

In an efort to ban all nuclear tests, a large majority at the United Nations General Assembly in New York passed the comprehensive test ban treaty (CTBT) in September, 1996. Although 180 states signed the treaty, only 145 ratified it, prohibiting the treaty from entering into force (CTBTO, 2008). The US Department of Energy detonated a 1.5 kiloton chemical explosive charge at the Nevada test site on September 22$^{\text{nd}}$, 1993. The experiment, named the non-proliferation experiment (NPE), was conducted in anticipation of the CTBT. The explosion was recorded by over 50 broadband seismic stations in the western United States (Tinker and Wallace, 1997). Scientists used these recordings and other measurements to learn to distinguish between nuclear and chemical explosions (Carr, 1994).

A less well known recording was made by the Subsurface Exploration Company of Pasadena, CA, which operated a 610-channel petroleum-exploration seismic array approximately 200 km distant. The array was oriented east-west in Railroad Valley, Nevada, which is located north of the Nevada Test Site, see Figure 1. This sign-bit equipment was activated at midnight and recorded an extraordinary coda over 5 minutes in length. The incoming waves are spatially coherent at early times, when all energy comes in as a single plane wave (see Figure 2a). Very rapidly after the first break, the wavefield becomes more chaotic, and at later arrivals the higher frequencies are lost, as observed in Figures 2b - 2d. At later times, recorded arrivals are incident for a large range of apparent slownesses. This phenomenon was studied by de Ridder (2008), who concluded that all admissible slownesses define a cone in the frequency-wavenumber domain, as seen in Figure 3. The slope of the cone is determined by the event with the slowest possible apparent velocity; a surface-wave traveling purely along the array.

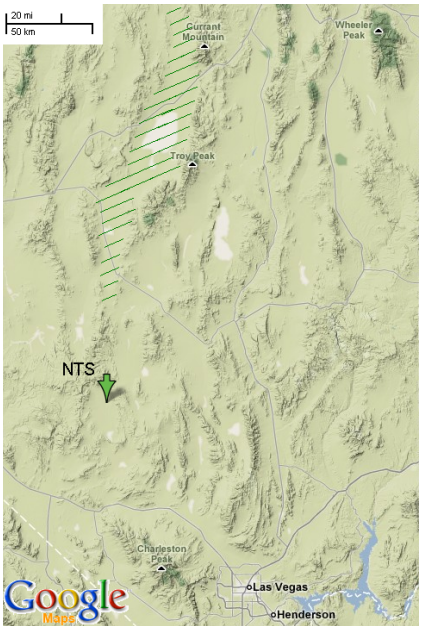

Figure 1: Map showing the location of the Nevada Test Site (arrow) and Railroad Valley (shaded area). [**NR**]

In this report, the coda of the NPE is studied using cross-correlation techniques. Two approaches are contrasted: the seismic interferometry (SI) method which potentially retrieves the full impulse response of the earth from the recorded background field (Wapenaar, 2004) and the spatial auto-correlation (SPAC) method, which retrieves dispersion curves of the fundamental mode of the surface-waves in a horizontally layered medium (Aki, 1957).

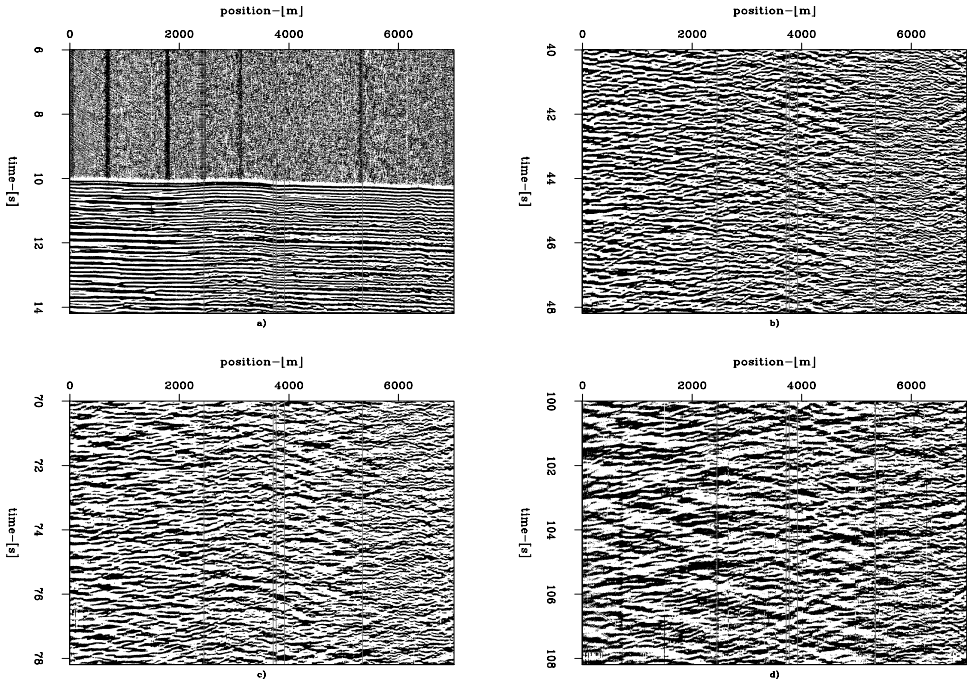

Figure 2: Four segments of the first NPE recording; a) segment containing the first arrival; b) segment 30 seconds after the first arrival; c) segment 60 seconds after the first arrival; d) segment 90 seconds after the first arrival. [**ER**]

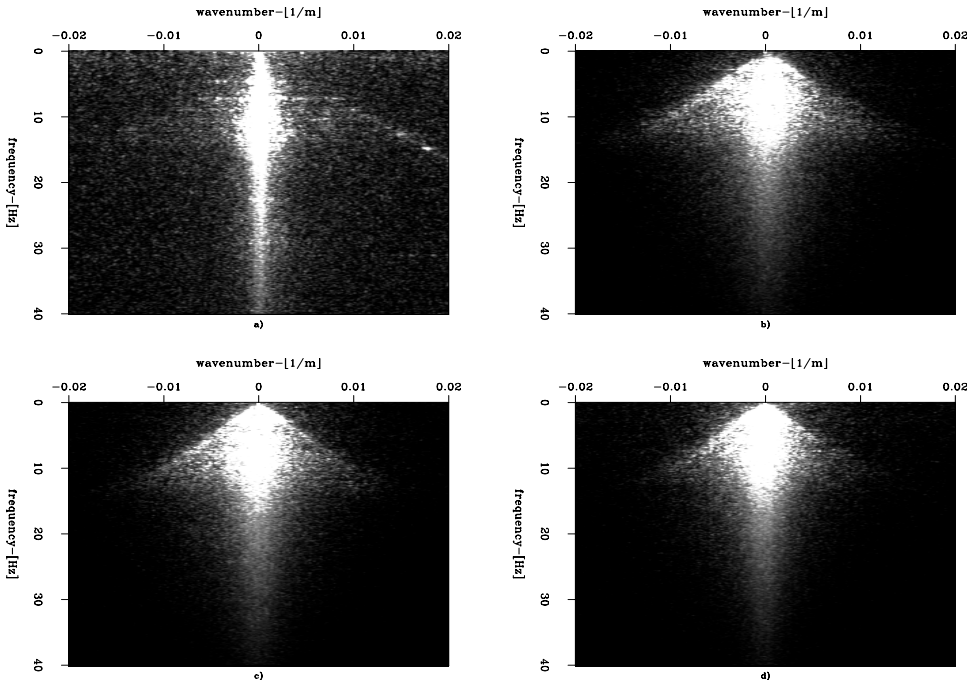

Figure 3: Frequency-wavenumber spectra of the NPE recording, subfigures a, b, c and d display each the frequency-wavenumber spectra for the corresponding subfigures in Figure 2. [**ER**]

SEISMIC INTERFEROMETRY AND THE SPATIAL AUTO-CORRELATION METHOD

Seismic interferometry refers to the principle of generating new seismic responses through cross-correlations of recorded seismic wavefields at receivers (Schuster, 2001). The first to derive this principle for deterministic wavefields in 1D media was Claerbout (1968), who showed that the reflection response of a 1D medium could be synthesized from the auto-correlation of the transmission response. Later derivations include many different approaches based upon: diffusivity of the wavefields (Weaver and Lobkis, 2001; Roux et al., 2005; Sánchez-Sesma et al., 2006; Sánchez-Sesma and Campillo, 2006), stationary phase analysis (Schuster et al., 2004; Snieder, 2004) and propagation invariants and reciprocity theorems (Claerbout, 1976; Weaver and Lobkis, 2004; Wapenaar, 2004; Wapenaar and Fokkema, 2006; van Manen et al., 2005).

Wapenaar and Fokkema (2006) derives an interferometric representation of the Green's function from energy principles. Under certain conditions, this representation can be simplified to a direct cross-correlation between two receiver stations. Consider a domain $\mathbf{D}$ in an arbitrary, inhomogeneous medium enclosing two points $\mathbf{x}_A$ and $\mathbf{x}_B$, bounded by an arbitrarily shaped surface $\partial\mathbf{D}$ with outward pointing normal vector $\mathbf{n}$. The interferometric representation of the Green's function for the vertical component of particle velocity measured at $\mathbf{x}_A$ in response to a vertical force-impulse point-source acting at $\mathbf{x}_B$ is given in the frequency-domain as follows (Wapenaar and Fokkema, 2006):

$$2\Re\{\hat{G}^{v,f}_{3,3}(\mathbf{x}_A,\mathbf{x}_B,\omega)\} = \tag{1}$$
$$-\oint_{\partial\mathbf{D}}\left[\hat{G}^{v,h}_{3,ij}(\mathbf{x}_B,\mathbf{x},\omega)\left\{\hat{G}^{v,f}_{3,i}(\mathbf{x}_A,\mathbf{x},\omega)\right\}^{*}+\hat{G}^{v,f}_{3,i}(\mathbf{x}_B,\mathbf{x},\omega)\left\{\hat{G}^{v,h}_{3,ij}(\mathbf{x}_A,\mathbf{x},\omega)\right\}^{*}\right]n_j\mathrm{d}^2\mathbf{x},$$

where the asterisk denotes complex conjugation, and ω denotes angular frequency. The notation convention for Green's functions is that superscripts denote the receiver (first) and source type (second), and subscripts denote the components of the source (first) and receiver (second) fields. The fields and sources in the elastodynamic system are particle velocity $\boldsymbol{v}$, stress tensor $\boldsymbol{\tau}$ (used below), external volume force density $\mathbf{f}$, and external deformation rate density $\mathbf{h}$. Einstein's summation convention is applied on all repeated subscripts.

The interferometric integral in equation 1 represents the real part of the elastodynamic Green's function between two receiver stations located at A and B, as a summation of cross-correlations of independent measurements at the two receiver stations. (Independent measurements of responses of various source components and types located on a surface enclosing both receivers are required to evaluate this integral.) The integral can be modified to reflect the field configuration of the NPE, where the receivers are located just below the traction-free surface, that has $\mathbf{n} = (0, 0, 1)$. The domain integral is split into two segments, $\partial\mathbf{D}_0$ and $\partial\mathbf{D}_1$, which are the parts of the domain boundary that coincide with the traction-free surface and the remainder,

respectively. Thus the interferometric representation, equation 1, can be split into two parts:

$$
\begin{aligned}
&2\Re\{\hat{G}^{v,f}_{3,3}(\mathbf{x}_A,\mathbf{x}_B,\omega)\} = \qquad (2)\\
&-\oint_{\partial\mathbf{D}_1}\left[\hat{G}^{v,h}_{3,ij}(\mathbf{x}_B,\mathbf{x},\omega)\left\{\hat{G}^{v,f}_{3,i}(\mathbf{x}_A,\mathbf{x},\omega)\right\}^* + \hat{G}^{v,f}_{3,i}(\mathbf{x}_B,\mathbf{x},\omega)\left\{\hat{G}^{v,h}_{3,ij}(\mathbf{x}_A,\mathbf{x},\omega)\right\}^*\right] n_j \mathrm{d}^2\mathbf{x}\\
&-\oint_{\partial\mathbf{D}_0}\left[\hat{G}^{v,h}_{3,i3}(\mathbf{x}_B,\mathbf{x},\omega)\left\{\hat{G}^{v,f}_{3,i}(\mathbf{x}_A,\mathbf{x},\omega)\right\}^* + \hat{G}^{v,f}_{3,i}(\mathbf{x}_B,\mathbf{x},\omega)\left\{\hat{G}^{v,h}_{3,i3}(\mathbf{x}_A,\mathbf{x},\omega)\right\}^*\right] \mathrm{d}^2\mathbf{x}\ ,
\end{aligned}
$$

where $\mathbf{n} = (0,0,1)$ has been substituted into the integral segment over the traction-free surface, $\partial\mathbf{D}_0$. According to source-receiver reciprocity, the required response $\hat{G}^{v,h}_{3,i3}$ at the traction-free surface satisfies $\hat{G}^{v,h}_{3,i3}(\mathbf{x}_b,\mathbf{x},\omega) = \hat{G}^{\tau,f}_{i3,3}(\mathbf{x},\mathbf{x}_B,\omega) = 0$. Thus the second integral on the right hand side of equation 2 is equal to zero.

Following Wapenaar and Fokkema (2006), consider the situation when the medium outside $\mathbf{D}$ is homogeneous and when the wavefield is generated by many mutually uncorrelated sources located on $\partial\mathbf{D}_1$, acting simultaneously with a weighted power spectrum, $w(\mathbf{x})\hat{S}(\omega)$. The integral over $\partial\mathbf{D}_1$ in equation 2, can be evaluated by a direct cross-correlation between recordings of particle velocity at receiver stations A and B:

$$
2\Re\{\hat{G}^{v,f}_{3,3}(\mathbf{x}_A,\mathbf{x}_B,\omega)\}\hat{S}(\omega) \approx \frac{2}{\rho c_p}\left\langle\, \hat{v}_3(\mathbf{x}_A,\omega)\hat{v}^*_3(\mathbf{x}_B,\omega)\,\right\rangle_x , \qquad (3)
$$

where c_p is the P-wave velocity. Note that the weighting factor $w(\omega)$ has disappeared. The weighting factor depends on the local medium parameters and source types, as is discussed at length by Wapenaar and Fokkema (2006). The wavefield required to make this simplification is named equipartitioned or diffuse (Hennino et al., 2001; Sánchez-Sesma and Campillo, 2006). The spatial ensemble average $\langle\cdot\rangle_x$ over sources is usually evaluated using a sufficiently long recording. Secondary scattering can render the coda of the NPE sufficiently equipartitioned. But in the coda of the NPE, most of the coherent energy between the receivers resides in the surface-wave mode (de Ridder, 2008) and does not provide significant energy for imaging.

A similar situation occurs for earthquake tremor. Aki Aki (1957) developed a technique named the spatial auto-correlation method. The close relationship between SI and SPAC was reported by Yokoi and Margaryan (2008). Their steps are briefly repeated here to derive from equation 3 a relationship used in the SPAC method. For a wavefield dominated by the surface modes, the frequency-domain Green's function for the vertical component of particle velocity measured at $\mathbf{x}_A$ in response to a vertical force-impulse point-source acting at $\mathbf{x}_B$ is

$$
\hat{G}^{v,f}_{3,3}(\mathbf{x}_A,\mathbf{x}_B,\omega) \approx -\omega\sum_{n=0}^{\infty}\hat{m}_2(k_n,x_{3,A})\hat{m}_2(k_n,x_{3,B})J_0(k_n\left|\mathbf{x}_A-\mathbf{x}_B\right|), \qquad (4)
$$

where $\hat{m}_2$ is a normalized eigenfunction, and J_0 is a zero-order Bessel function of the first kind (Yokoi and Margaryan (2008) from Aki and Richards (2002)). Substituting

this Green's function into the left side of equation 3 expands it to

$$2\Re\left\{-\omega\sum_{n=0}^{\infty}\hat{m}_2(k_n,x_{3,A})\hat{m}_2(k_n,x_{3,B})J_0(k_n\left|\mathbf{x}_A-\mathbf{x}_B\right|)\right\}\hat{S}(\omega)\approx\frac{2}{\rho c_p}\left\langle\,\hat{v}_3(\mathbf{x}_A,\omega)\hat{v}_3^*(\mathbf{x}_B,\omega)\,\right\rangle_x. \tag{5}$$

Normalizing by the auto-correlation of the recording at station A gives

$$\frac{2\Re\left\{-\omega\sum_{n=0}^{\infty}\hat{m}_2(k_n,x_{3,A})\hat{m}_2(k_n,x_{3,B})J_0(k_n\left|\mathbf{x}_A-\mathbf{x}_B\right|)\right\}}{2\Re\left\{-\omega\sum_{n=0}^{\infty}\left\{\hat{m}_2(k_n,x_{3,A})\right\}^2J_0(0)\right\}}\approx\frac{\frac{2}{\rho c_p}\left\langle\,\hat{v}_3(\mathbf{x}_A,\omega)\hat{v}_3^*(\mathbf{x}_B,\omega)\,\right\rangle_x}{\frac{2}{\rho c_p}\left\langle\,\hat{v}_3(\mathbf{x}_A,\omega)\hat{v}_3^*(\mathbf{x}_A,\omega)\,\right\rangle_x}. \tag{6}$$

When the fundamental surface-wave dominates, and both receivers are located at equal depth ($x_{3,A}=x_{3,B}$), the higher-order terms can be neglected, and equation 6 simplifies to

$$J_0(k_0\left|\mathbf{x}_A-\mathbf{x}_B\right|)\approx\frac{\left\langle\,\hat{v}_3(\mathbf{x}_A,\omega)\hat{v}_3^*(\mathbf{x}_B,\omega)\,\right\rangle_x}{\left\langle\,\hat{v}_3(\mathbf{x}_A,\omega)\hat{v}_3^*(\mathbf{x}_A,\omega)\,\right\rangle_x}\approx\phi(\mathbf{x}_A,\mathbf{x}_B,\omega), \tag{7}$$

where $\phi(\mathbf{x}_A,\mathbf{x}_B,\omega)$ is defined as the azimuthally averaged auto-correlation coefficient. The wavenumber of the fundamental surface-wave mode is given by a specific dispersion curve, $k_0=\frac{\omega}{c(\omega)}$, where $c(\omega)$ is phase velocity.

Notice from equation 7 how the cross-spectra in frequency *and space* are predicted to obey Bessel functions, with oscillations determined by the phase velocity. The Bessel function of the first kind is real-valued. The cross-spectrum on the right hand-side is complex-valued, but if the conditions that lead to equation 7 are fulfilled, the imaginary component vanishes (Asten, 2006), ($\hat{v}_3(\mathbf{x}_A,\omega)\hat{v}_3^*(\mathbf{x}_A,\omega)$ is always real). The real part of the cross-spectrum is retrieved as the zero-lag temporal cross-correlation, i.e., a spatial auto-correlation coefficient. It should be noted that the close relationship between SI and SPAC seems to hold only for surface-waves in horizontally stratified media. The SPAC method as commonly applied involves fitting Bessel functions to the computed auto-correlation coefficient with frequency, with explicit directional averaging of the wavefield in all directions. In the case of isotropic wavefields, this averaging is unnecessary (Aki, 1957; Okada, 2003). The coda of the NPE quickly becomes isotropic after the first break, thus this relationship seems suitable for the cross-spectra calculated from NPE data. To introduce an estimation of attenuation, the Green's function, equation 4, is supplemented with an exponential attenuation factor $Q(\omega)$, (Aki and Richards, 2002). The final model for the frequency-domain spatial auto-correlation coefficient $\phi(\mathbf{x}_A,\mathbf{x}_B,\omega)$ becomes

$$\phi(\mathbf{x}_A,\mathbf{x}_B,\omega)=J_0\left(\frac{\omega}{c(\omega)}\left|\mathbf{x}_A-\mathbf{x}_B\right|\right)\,\exp\left\{-\frac{\omega}{c(\omega)}\frac{1}{2Q(\omega)}\left|\mathbf{x}_A-\mathbf{x}_B\right|\right\}. \tag{8}$$

DATA ANALYSIS

The two records analyzed are of approximately 131 seconds duration (2^{14} samples at a 125 Hz sampling frequency) at 610 stations with a 45-foot spacing. The second

recording starts a few seconds after the first recording ends. Although the exact location of the NPE array is unknown, the data shows that the first 66 stations were located at an angle with respect to the other stations. Starting from station 67 located at 0 m in Figure 2, 512 stations are analyzed. The first arrivals were muted from the first record. All records were filtered in the frequency-wavenumber domain with a high-cut cosine filter centered around an angle corresponding to a velocity of 770 m/s, determined from Figure 3. This removes noise from the coda and interpolates the missing traces. For velocities smaller and equal to 770 m/s this did not affect the estimation of the surface wave velocity as described below.

The spectrum at each station was estimated using a multitaper spectral-estimation technique. This provides several statistically independent estimates of the spectrum and decreases spectral leakage (Prieto et al., 2007, 2008b). In this procedure, a time record with N samples is first multiplied with a set of K orthogonal Slepian tapers (Thomson, 1982). Second, the discrete Fourier transformation is computed for each tapered trace as follows:

$$x^k(\omega) = \sum_{t=0}^{N-1} x(t)\nu^k(t)\exp\left\{-i\omega t\right\}, \tag{9}$$

where the k^{th} Slepian taper is denoted by $\nu^k(t)$. The cross-spectrum $\rho(\omega)$ between two traces x and y is calculated from the spectral estimations $x^k(\omega)$ and $y^k(\omega)$ according to

$$\rho(\omega) = \sum_{k=1}^{K} x^k(\omega)\left\{y^k(\omega)\right\}^*. \tag{10}$$

Interferometric gathers in the frequency-domain are computed by consecutively selecting each station in the array as a master station and computing the cross-spectra between all other stations and this master station. The collection of interferometric gathers is further analyzed in the midpoint-offset domain (m, h). To enhance the signal-to-noise ratio, the retrieved gathers are smoothed over 50 midpoints, corresponding to a length of 680 m.

We first study the result from processing the records in the time domain, as is common in seismic interferometry practices. A common-midpoint section at $m =$ 5144 m is given in Figure 4, and a common-offset section for $h = 261$ m is given in Figure 5. de Ridder (2008) did not observe any event, besides the surface-wave events intersecting each other at $(h, t) = (0, 0)$ that is coherent across different midpoints. When we study the common-offset section in Figure 5, we can see the arrival time of the surface wave event at ~ 0.5 s slightly varying with offset. If we neglect this and assume the earth is horizontally layered, the recovered gathers can be stacked over common-offsets as shown in Figure 6. Estimating the slope of the event visible in Figures 4 and 6, de Ridder (2008) found a velocity of $c_r = 770$ m/s. The subscript r refers to a Rayleigh wave, which is the dominant surface-wave type recorded in the vertical component of particle velocity in groundroll. It is difficult to extract more information from the time-domain images. Additional analysis of the retrieved

gathers can be performed in the frequency-domain, by inverting for phase velocity and attenuation factors. The frequency-domain equivalents of the time-domain gathers in Figures 4 and 6 are shown respectively in Figures 7 and 9.

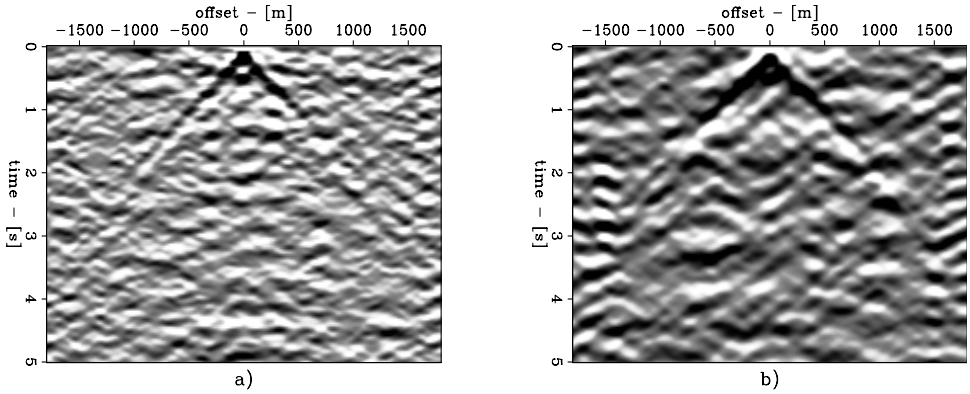

Figure 4: Interferometric common-midpoint gather gather, at $m = 5144$ m; a) retrieved from recording 1, b) retrieved from recording 2. [**ER**]

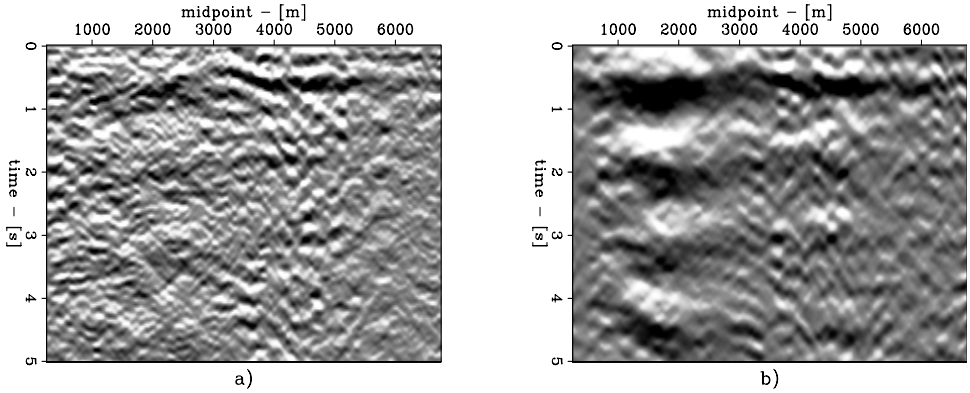

Figure 5: Interferometric common-offset gather, for $h = 261$ m; a) retrieved from recording 1, b) retrieved from recording 2. [**ER**]

INVERSION FOR DISPERSION CURVES

In Figures 7 and 9, Bessel functions are clearly observed at different oscillation periods for different frequencies. Moreover, from Figure 5 it can be concluded that the period of oscillation of the Bessel functions should not remain constant for all gathers along the array. We use our model stated in equation 8 to estimate phase velocity and attenuation from retrieved frequency-domain common-midpoint gathers. This analysis can be repeated for all gathers at all midpoints, thereby detecting variation in dispersion curves along the array.

The optimization procedure is done by a grid-search for the two dimensions in the model space for each frequency. The inversion for phase velocity $c(\omega)$ is fairly well

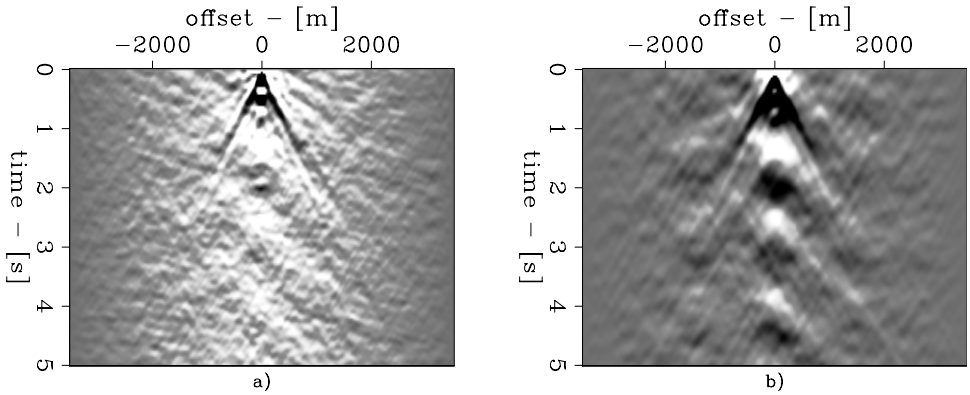

Figure 6: Common-offset stack for the interferometric gathers; a) retrieved from recording 1, b) retrieved from recording 2. [**ER**]

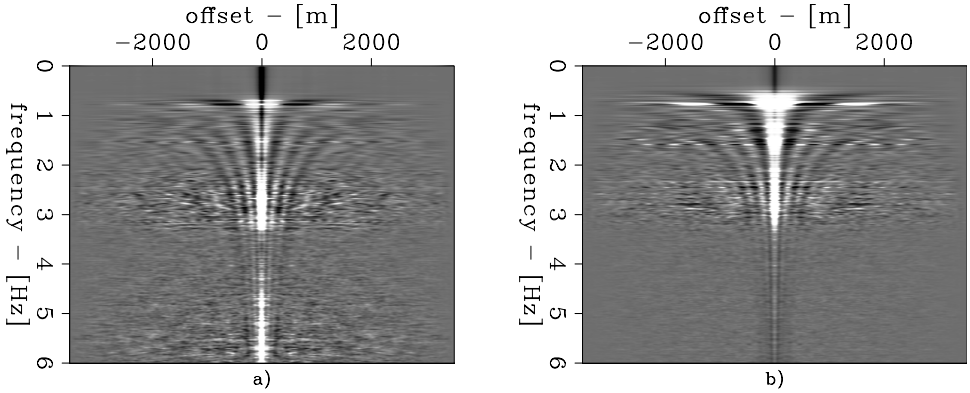

Figure 7: Frequency-domain common-offset stack; a) retrieved from recording 1, b) retrieved from recording 2. [**ER**]

posed because of the zero crossings of the Bessel function; in a second step the decay rate observed in the gathers is inverted for an attenuation factor $Q(\omega)$. The division of the cross-spectrum by the auto-correlation of the recording at station A is very unstable, and is avoided by multiplication of equation 8 with the auto-correlation of the recording at station A.

An example in which theory matches the data reasonably well is at midpoint $m = 5144$ m. In Figure 8, the cross-spectrum for this midpoint and at 2.4 Hz calculated from recording 1 and 2 are shown together with the fitted Bessel and damped Bessel functions. The estimated phase velocities and attenuation factors are $c(4.8\pi) = 560$ m/s from recording 1, and $Q(4.8\pi) = 22.3$ and $c(\omega) = 562$ m/s, $Q = 17.8$ from recording 2.

This analysis is performed for all frequencies and on both recordings. The cross-spectrum calculated at midpoint $m = 5144$ m for all frequencies from recording 1 and 2 are shown in Figure 9. The best fit of Bessel functions to the midpoint-gathers in Figure 9 are shown in Figure 10 and the best fit of damped Bessel functions to

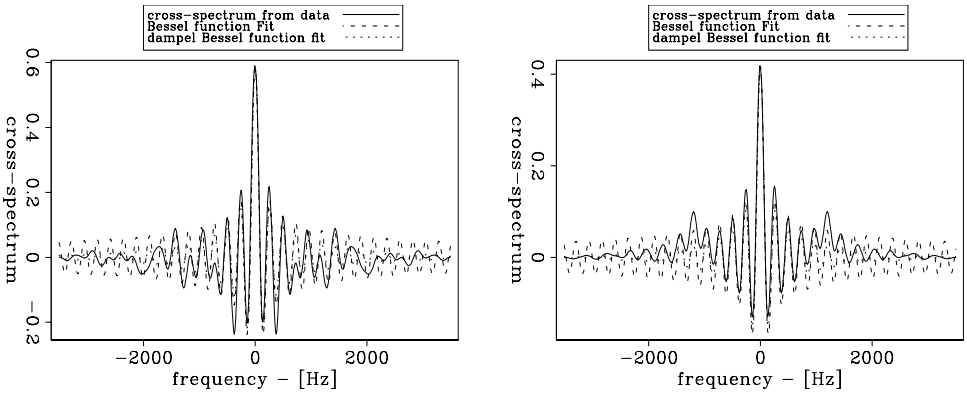

Figure 8: Cross-spectrum at 2.4 Hz at midpoint $m = 5144$ m; a) retrieved from recording 1, b) retrieved from recording 2. Included are the fitted Bessel and damped Bessel functions, from recording 1; $c(4.8\pi) = 560$ m/s, $Q(4.8\pi) = 22.3$, from recording 2; $c(4.8\pi) = 562$ m/s, $Q(4.8\pi) = 17.8$. [**ER**]

the midpoint gathers in Figure 10 are shown in Figure 11. The estimated dispersion curves and attenuation factors for the midpoint gather at $m = 5144$ m are shown in Figure 12. The dispersion curves estimated for all midpoints from recording 1 and 2 are shown together in Figure 13. The dispersion curves range from values twice as large as the estimated group velocity of 770 m/s to velocities slightly smaller than the estimated group velocity. Although there are some spurious estimated phase velocities, a clear trend can be seen towards the right side of the array for generally higher phase velocities. The estimated attenuation coefficients vary much more strongly and become seemingly more incoherent with frequency. For the midpoint gather at $m = 5144$ m and the frequency band of 1 to 3 Hz, the attenuation factor seems to be in the range of $Q = 5$ to $Q = 30$.

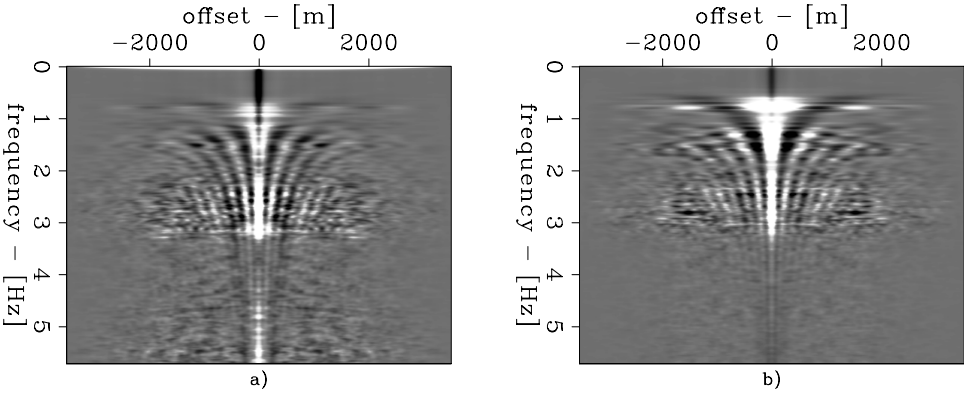

Figure 9: Cross-spectra calculated from recording 1, in a) and 2 in b) at $m = 5144$ m. [**ER**]

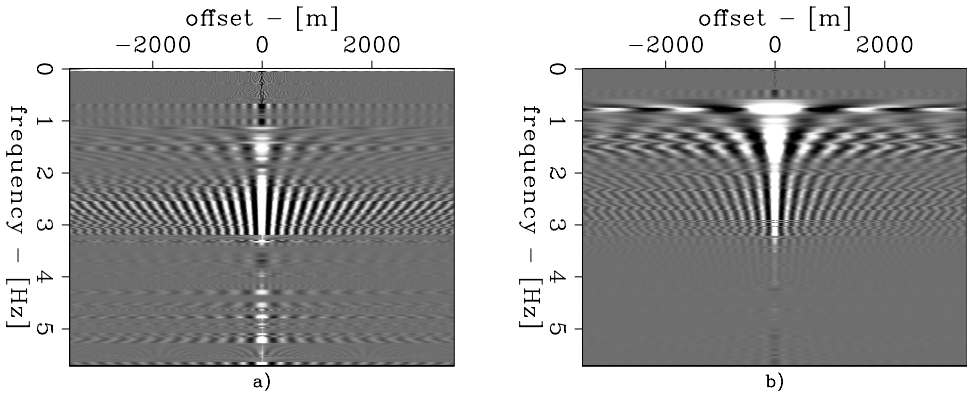

Figure 10: Bessel functions fitted to the cross-spectra calculated from recording 1, in a) and 2 in b), at $m = 5144$ m. The estimated phase velocity curves are shown in Figure 12. [**ER**]

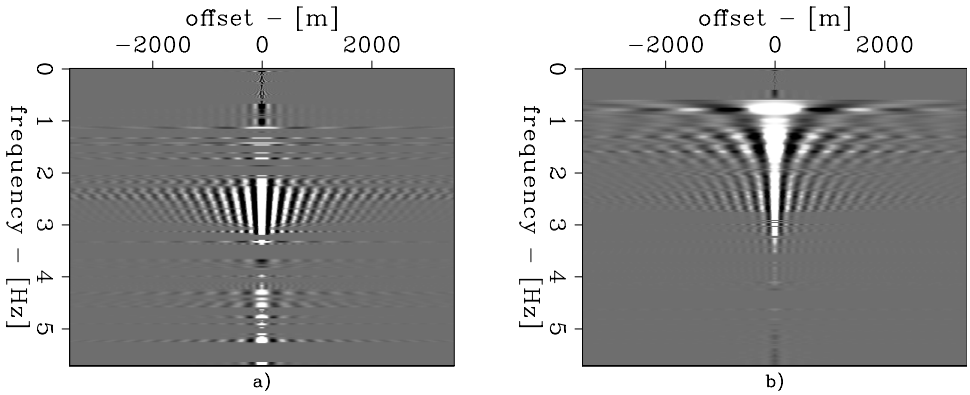

Figure 11: Damped Bessel functions fitted to the cross-spectra calculated from recording 1, in a) and 2 in b), at $m = 5144$ m. The estimated attenuation factors are shown in Figure 12. [**ER**]

DISCUSSION AND CONCLUSIONS

Consistent with the observation of de Ridder (2008), we have observed that the cross-spectra of the NPE coda contain coherent energy that corresponds to the surface-wave. This observation shows that for the coda of the NPE, the SI approach is analogous to the SPAC approach. Both methods provide different information; in addition to an estimate of group velocity for the surface wave from SI, we have also estimated phase velocity from the cross-spectra. Only the energy between 1 and 4 Hz can be fitted unambiguously with J_0 functions, because higher frequencies contain too much spurious energy that is not equipartitioned, and lower frequencies do not contain sufficient energy. We also show that by analysing common-midpoint gathers, we can begin to see spatial variation of phase velocities along the array. This suggest the possibility to study 3D structure using cross-correlation techniques, as has also been proposed by Harmon et al. (2008) and Prieto et al. (2008a).

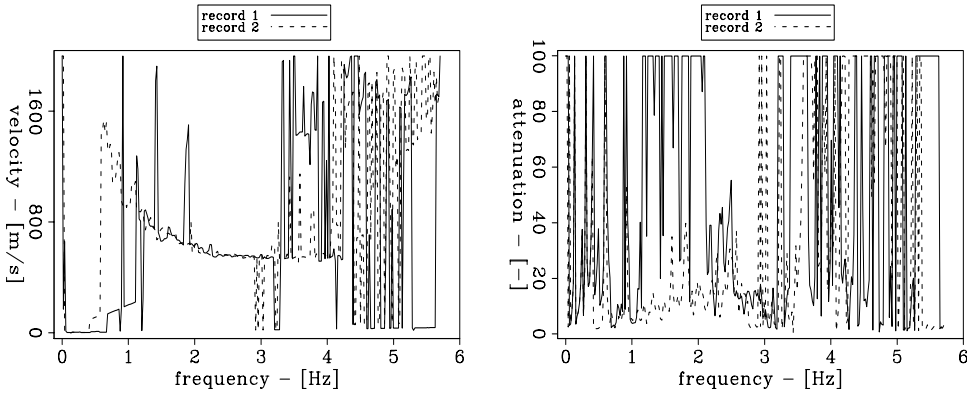

Figure 12: Dispersion curve and attenuation factors estimated from the cross-spectra at $m = 5144$ m calculated from recordings 1 and 2. [**ER**]

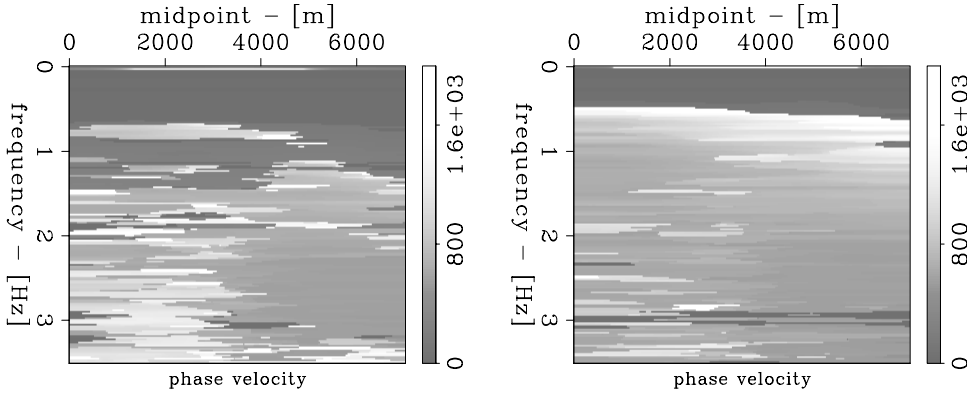

Figure 13: Estimated phase velocity from the cross-spectra calculated along the array. A clear trend of increasing phase velocities to the right-side can be observed. [**CR**]

The relatively accurate fit of the damped Bessel function for Figure 8 suggests that most of the energy is part of the fundamental mode of the surface wave. Small discrepancies can be explained by many factors; the energy might not be completely equipartitioned, there could be some energy in higher modes, and very likely there are heterogeneities on a scale smaller than the smoothing length that invalidate our assumptions of a horizontally layered earth. Another effect of scattering is attenuation (Hong et al., 2005). The effects of scattering attenuation and intrinsic attenuation are not easily distinguishable at this point and further research is needed.

The source position of the NPE, transversely oriented to the direction of the array, seems very unfavorable for SI or SPAC. But small-scale heterogeneities in the earth rendered the coda wavefield equipartitioned to first order. Since the recording is sign-bit, this property is fully exploited, because amplitude changes with azimuth are suppressed. Moreover, the energy is relatively well distributed in both directions along the array, since the array is nearly transverse with respect to NTS.

Although the wavefield does not contain sufficient energy for imaging, subsurface

information can still be extracted by inverting the dispersion curves for a subsurface velocity profile. The recording of the NPE and geometry of the array in Railroad Valley provided the rare opportunity to study the properties of a small earthquake-like event in the transverse direction, with high spatial resolution.

ACKNOWLEDGMENTS

The author thanks Germán Prieto for many discussions on Green's function retrieval and his multitaper spectrum analysis Fortran library, Jon Claerbout for his continuing encouragement to investigate this dataset and John Vidale for supplying the data tape file.

REFERENCES

Aki, K., 1957, Space and time spectra of stationary stochastic waves, with special reference to microtremors: Bulletin of the Earthquake Research Institute, **35**, 415–456.

Aki, K. and P. G. Richards, 2002, Quantitative Seismology - second edition: University Science Books.

Asten, M. W., 2006, On bias and noise in passive seismic data from finite circular array data processed using spac methods: Geophysics, **71**, V153–V162.

Carr, D. B., 1994, Non-proliferation experiment recorded at the pinedale seismic research facility: Sandia National Laboratories.

Claerbout, J. F., 1968, Synthesis of a layered medium from its acoustic transmission response: Geophysics, **33**, 264–269.

———, 1976, Fundamentals of geophysical data processing; with applications to petroleum prospecting: Blackwell Scientific Publications.

CTBTO, 2008, CTBTO Preparatory Commission: http://www.ctbto.org/. (last visited: Oktober 15, 2008).

de Ridder, S., 2008, Spectral analysis of the non-proliferation experiment: Technical report, SEP-134.

Harmon, N., P. Gerstoft, C. A. Rychert, G. A. Abers, M. S. de la Cruz, and K. M. Fischer, 2008, Phase velocities from seismic noise using beamforming and cross correlation in costa rica and nicaragua: Geophys. Res. Let., **35**, L19303–1–L19303–6.

Hennino, R., N. Trégourès, N. M. Shapiro, L. Margerin, M. Campillo, B. A. van Tiggelen, and R. L. Weaver, 2001, Observation of equipartition of seismic waves: Physical Review Letters, **86**, 3447–3450.

Hong, T.-K., R.-S. Wu, and B. L. N. Kennett, 2005, Stochastic features of scattering: Physics of the Earth and Planetary Interiors, **148**, 131–148.

Okada, H., 2003, The microtremor survey method. Geophysical Monograph, No. 12: Society of Exploration Geophysicists.

Prieto, G. A., J. F. Lawrence, and G. C. Beroza, 2008a, Anelastic earth structure from the coherency of the ambient seismic field. submitted to J. Geophys. Res.

Prieto, G. A., R. L. Parker, and F. L. Vernon, 2008b, A Fortran 90 library for multitaper spectrum analysis. Accepted in Computers and Geosciences.

Prieto, G. A., D. J. Thomson, F. L. Vernon, P. M. Shearer, and R. L. Parker, 2007, Confidence intervals of earthquake source parameters: Geophys. J. Int., **168**, 1227–1234.

Roux, P., K. G. Sabra, W. A. Kuperman, and A. Roux, 2005, Ambient noise cross correlation in free space: Theoretical approach: JASA, **117**, 79–84.

Sánchez-Sesma, F. J. and M. Campillo, 2006, Retrieval of the Green's function from cross correlation: The canonical elastic problem: Bull. Seism. Soc. Am., **96**, 1182–1191.

Sánchez-Sesma, F. J., J. A. Párez-Ruiz, M. Campillo, and F. Luzón, 2006, Elastodynamic 2d Green's function retrieval from cross-correlation: Canonical inclusion problem: Geophys. Res. Let., **33**, L13305–1–L13305–6.

Schuster, G. T., 2001, Theory of daylight/interferometric imaging - tutorial: 63rd Meeting, European Associated of Geoscientists and Engineers, Expanded Abstracts, Session A32, Expanded Abstracts, A32.

Schuster, G. T., J. Yu, J. Sheng, and J. Rickett, 2004, Interferometric/daylight seismic imaging: Geophys. J. Int., **157**, 838–852.

Snieder, R. K., 2004, Extracting the Green's function from the correlation of coda waves: A derivation based on stationary phase: Phys. Rev. E, **69**, 046610–1–046620–8.

Thomson, D. J., 1982, Spectrum estimation and harmonic analysis: Proceedings of the IEEE, **70**, 1955–1996.

Tinker, M. A. and T. C. Wallace, 1997, Regional phase development of the non-proliferation experiment within the Western United States: Bull. Seism. Soc. Am., **87**, 383–395.

van Manen, D.-J., J. O. A. Robertsson, and A. Curtis, 2005, Modeling of wave propagation in inhomogeneous media: Phys. Rev. Lett., **94**, 164301–1–164301–4.

Wapenaar, K., 2004, Retrieving the elastodynamic Green's function of an arbitrary inhomogeneous medium by cross correlation: Phys. Rev. Lett., **93**, 254301–1 – 254301–4.

Wapenaar, K. and J. Fokkema, 2006, Green's function representations for seismic interferometry: Geophysics, **71**, SI33–SI46.

Weaver, R. L. and O. I. Lobkis, 2001, Ultrasonics without a source: Thermal fluctuation correlations at mhz frequencies.: Phys. Rev. Let., **87**, 134301–1 – 134301–4.

———, 2004, Diffuse fields in open systems and the emergence of the Green's function (L): J. Acoust. Soc. Am., **116**, 2731–2734.

Yokoi, T. and S. Margaryan, 2008, Consistency of the spatial autocorrelation method with seismic interferometry and its consequence: Geophysical Prospecting, **56**, 435–451.